

25 Abstract

26 Projections of the winter North Atlantic circulation exhibit large spread. Coupled Model
27 Intercomparison Project archives typically provide only a few ensemble members per model,
28 rendering it difficult to quantify reducible model structural uncertainty and irreducible internal
29 variability (IV) in projections. We estimate using the Multi-Model Large Ensemble Archive that
30 model structural differences explain two-thirds of the spread in late 21st century (2080-2099)
31 projections of the winter North Atlantic Oscillation (NAO). This estimate is biased by systematic
32 model errors in the forced NAO response and IV. Across the North Atlantic, the NAO explains a
33 substantial fraction of the spread in mean sea level pressure (MSLP) projections due to IV,
34 except in the central North Atlantic. Conversely, the spread in North Atlantic MSLP projections
35 associated with model differences is largely unexplained by the NAO. Therefore, improving
36 understanding of the NAO alone may not constrain the reducible uncertainty in North Atlantic
37 MSLP projections.

38

39 Plain Language Summary

40 Variations in atmospheric circulation over the North Atlantic in winter are dominated by the
41 North Atlantic Oscillation (NAO) pattern, which has a strong influence on regional climate and
42 is often associated with severe weather events. It is uncertain how the NAO will respond to
43 future changes in climate driven by human activity. This uncertainty in future projections has
44 two main sources, which are yet to be fully quantified: first, there are large natural variations in
45 the NAO on the timescale of many decades, which can mask the effect of long-term climate
46 change on the NAO; second, different climate models have different representations of physical
47 processes, which can lead to differences in the future climates they simulate. Here we estimate,
48 using an unprecedented number of simulations from different climate models, that model
49 structural differences explain the majority of uncertainty in late 21st century NAO projections.
50 This result is important because it suggests that uncertainty in NAO projections could be reduced
51 with improved knowledge of the physical processes involved. However, the NAO itself does not
52 explain much of the model structural uncertainty in regional sea level pressure projections in and
53 around the North Atlantic basin, suggesting other dynamical processes must be understood.

54 **1 Introduction**

55 The North Atlantic atmospheric circulation has a strong influence on Northern
56 Hemisphere regional climate and is often associated with severe weather events (Buehler et al.,
57 2011; Hurrell et al., 2003). For a given future greenhouse gas and aerosol forcing scenario,
58 previous studies have found substantial spread in projections of late 21st century North Atlantic
59 circulation change across models from the Coupled Model Intercomparison Project Phases 5 and
60 6 (CMIP5 and CMIP6; Collins et al., 2013; Oudar et al., 2020; Shepherd, 2014; Zappa et al.,
61 2018). The model spread partly arises from competing large-scale drivers, such as upper and
62 lower tropospheric temperature gradient changes (Harvey et al., 2014) and stratospheric
63 circulation (Manzini et al., 2014; Simpson, Hitchcock, et al., 2018), with the relative dominance
64 of each factor differing across models (Zappa & Shepherd, 2017).

65 The extent to which the spread in multi-model projections of the North Atlantic
66 circulation is from model structural differences versus internal climate variability (IV) remains
67 an open question. This is partly because models contributing to CMIP5/6 typically only provide
68 a small number of realisations with different initial conditions and the same external forcing to
69 sample IV. This makes it difficult to quantify the contributions of model structural uncertainty
70 and IV to the spread in projections without making assumptions (e.g., approximating 21st century
71 IV using IV in a stationary pre-industrial climate; Hawkins & Sutton, 2009).

72 This study aims to advance understanding of the roles of model structural error and IV in
73 North Atlantic circulation projections. To achieve this, we use the recently available Multi-
74 Model Large Ensemble Archive (MMLEA; Deser et al., 2020) and data from CMIP5/6. We
75 focus on the leading mode of variability in the North Atlantic circulation – the North Atlantic
76 Oscillation (NAO) – which is associated with changes in the strength and latitude of the eddy-
77 driven jet (Woollings et al., 2010). To guide our investigation, we address the following
78 questions:

- 79 1. What are the relative contributions of IV and model structural uncertainty to spread in
80 NAO projections?
- 81 2. When do the forced NAO response and model differences in this response emerge from
82 IV in the 21st century?

- 83 3. What is the minimum number of ensemble members required to separate the forced NAO
84 response, and model differences in this response, from IV?
85 4. To what extent is spread in North Atlantic circulation projections explained by the NAO?

86 Addressing these questions will aid the interpretation of North Atlantic circulation projections,
87 improving their utility, and provide guidance for designing future model experiments.

88

89 **2 Methods**

90 2.1 Datasets

91 The MMLEA contains large (16-100 member) initial-condition ensembles for 7
92 comprehensive climate models (Table S1; Hazeleger et al., 2010; Jeffrey et al., 2013; Kay et al.,
93 2015; Kirchmeier-Young et al., 2017; Maher et al., 2019; Rodgers et al., 2015; Schlunegger et
94 al., 2019; Sun et al., 2018). We use historical and Representative Concentration Pathway
95 (RCP)8.5 simulations from the MMLEA models for the common period 1950-2099. RCP8.5 was
96 chosen because only a small subset of the models is available for other RCPs. Since GFDL-
97 ESM2M and GFDL-CM3 have similar atmosphere, ocean, sea-ice and land components (Maher
98 et al., 2021), and give similar results, we discard the smaller GFDL-CM3 ensemble from the
99 MMLEA analysis. The winter North Atlantic circulation is described using monthly mean sea
100 level pressure (MSLP) data averaged over December to February (DJF). Following Collins et al.
101 (2013), the long-term climate response is computed as the 20-year epoch difference between a
102 future period and a near-present-day period (updated to 1995-2014; year is for January).

103 We also use historical and RCP8.5 simulations from 39 CMIP5 models (Taylor et al.,
104 2012), and historical and Shared Socioeconomic Pathway (SSP)5-8.5 simulations from 36
105 CMIP6 models (Eyring et al., 2016); Table S2. The forcing scenarios changed in CMIP6, where
106 SSP5-8.5 has the most similar total end-of-century radiative forcing to RCP8.5 (Meinshausen et
107 al., 2020). However, there are differences in the mix of forcings between the RCP and SSP
108 scenarios (Meinshausen et al., 2011, 2020) to be borne in mind when comparing results.

109 Generally, only a few ensemble members are available for the CMIP5/6 simulations, so
110 we estimate IV using the pre-industrial control (piControl) runs. Model drift is eliminated by
111 subtracting each run’s long-term linear trend. Various observation-based datasets are used to
112 evaluate the spread in model projections against observed IV. Since multi-decadal timescales are
113 our focus, we use two centennial-scale reanalysis datasets: the NOAA-CIRES-DOE 20th Century
114 Reanalysis version 3 (20CRv3; Compo et al., 2011; Slivinski et al., 2019) and the ECMWF 20th
115 Century Reanalysis (ERA20C; Poli et al., 2016). An 1000 member “Observational Large
116 Ensemble” (Obs LE; McKinnon & Deser, 2018) is also used, which contains synthetic historical
117 trajectories produced by a statistical model based on observed climate statistics. We use the full
118 extent of Obs LE (1921-2014), and the longer common period of 1900-2010 for 20CRv3 and
119 ERA20C to minimise sampling issues. Forced trends in 20CRv3 and ERA20C are estimated and
120 removed using linear least squares regression; Obs LE by construction has no forced MSLP trend
121 (McKinnon & Deser, 2018).

122 All model and observation-based data were bilinearly interpolated onto a common 2°
123 horizontal grid; this procedure does not alter our results.

124 2.2 NAO definition

125 Following Stephenson et al. (2006) and Baker et al. (2018), the NAO index is defined as
126 the difference in area-averaged MSLP between a southern box (90W-60E, 20N-55N) and a
127 northern box (90W-60E, 55N-90N) in the North Atlantic. This index is less sensitive to
128 differences in centres of action between observations and models than the station-based index
129 (Hurrell et al., 2003; Stephenson et al., 2006), and is also less variable enabling easier detection
130 of a forced NAO response from IV. Furthermore, it is less affected by issues of interpretability
131 that occur when using a mathematically constructed EOF-based index (Ambaum et al., 2001;
132 Dommenges & Latif, 2002; Stephenson et al., 2006).

133 Each MMLEA model’s historical NAO pattern (Figure S1) is constructed from the
134 regression slopes obtained by regressing historical (1951-2014) timeseries of DJF MSLP at each
135 grid-point onto the NAO index timeseries; using a future period gives similar results. All
136 timeseries are first linearly detrended. The pattern is defined separately for each ensemble
137 member and then the ensemble mean is calculated (Simpson et al., 2020). The NAO-congruent

138 part of an MSLP anomaly map is obtained by multiplying the historical NAO pattern by the
 139 NAO index anomaly. Figure S1 also shows observation-based and CMIP5/6 multi-model mean
 140 (MMM) historical NAO patterns; largely, the modelled and observation-based patterns are
 141 highly correlated.

142 2.3 Statistical methods

143 In each MMLEA model, uncertainty due to IV is mainly estimated as the standard
 144 deviation across ensemble members (Deser et al., 2012). The externally forced response is
 145 estimated using the ensemble mean. The percentage variance contribution of IV (% U_{IV}) and of
 146 model structural differences (% U_{MD}) to the total uncertainty in MMLEA projections is quantified
 147 following Maher et al. (2021; Text S1).

148 A forced response is described as “robust” if it is statistically detectable from IV at the
 149 95% confidence level. Two-sided confidence intervals for a forced response (μ) are calculated as
 150 $\mu \pm t\sigma/\sqrt{N}$ (von Storch & Zwiers, 1999). t is the Student’s t-distribution value for $p=0.025$ and
 151 $N-1$ degrees of freedom, σ is the inter-member standard deviation of the epoch difference, and N
 152 is the ensemble size.

153 To estimate the minimum ensemble size (N_{\min}) required to detect a robust forced NAO
 154 index response of a given magnitude (X) between any two 20-year epochs, we follow Screen et
 155 al. (2014) and re-arrange a two-sided Student’s t-test for a difference of means (Text S2):

$$156 N_{\min} = 2t_c^2 \times (\sigma/X)^2.$$

157 t_c is for $p=0.025$ and $2N_{\min}-2$ degrees of freedom, and σ is the standard deviation of 20-year
 158 epoch means due to IV. N_{\min} is calculated for a difference in forced response (X) where σ is for
 159 differences in 20-year means.

160

161 3 Results

162 Figure 1 shows winter NAO index anomalies between 2080-2099 and 1995-2014 in the
 163 CMIP6, CMIP5 and MMLEA models. For both CMIP5/6 ensembles, the MMM response in the

164 NAO index is ~ 1.5 hPa. However, the MMM responses are generally small compared to the
165 spread across the individual models. While some models have large positive NAO anomalies
166 exceeding their modelled range of IV, most modelled anomalies are smaller than IV. The range
167 of NAO anomalies is 6 hPa in CMIP6 and 7 hPa in CMIP5 – comparable to the observed range
168 of NAO variability (Figure 1, grey box) – where 86% and 79% of models agree on sign
169 respectively.

170 Given many CMIP5/6 models only have one ensemble member available, it is impossible
171 to separate the spread in projections into parts due to structural model differences and IV.
172 Despite this limitation, uncertainty in projections is often examined using these models (e.g.,
173 Hawkins & Sutton, 2009). The MMLEA models suggest there are indeed substantial inter-model
174 differences in the forced response of up to 5 hPa (Figure 1, coloured circles). Using Maher et al.
175 (2021)'s uncertainty decomposition, we find that model structural differences and IV contribute
176 to 66% and 34%, respectively, of the total uncertainty in MMLEA NAO projections. The
177 following sections examine each source of uncertainty in detail.

178 3.1 Uncertainty from internal variability

179 In several MMLEA models, the forced winter NAO response is smaller than IV as
180 measured by the ensemble spread (Figure 1). Using the ensemble spread to assess the range of
181 possible futures assumes that the models adequately represent observed NAO variability.
182 However, as in previous studies (Bracegirdle et al., 2018; Kim et al., 2018; Kravtsov, 2017;
183 Simpson, Deser, et al., 2018; Wang et al., 2017), we find that most CMIP5/6 and MMLEA
184 models underestimate low frequency NAO variability compared to observation-based datasets
185 (Figure 1, black whiskers versus grey lines; Tables S1-S2). The model projections may therefore
186 be overconfident: i.e., a larger part of the uncertainty in the future real-world NAO response may
187 be from IV. When model-based estimates of IV are adjusted to an observation-based estimate
188 (Text S1), IV and model structural differences each contribute to half of the total uncertainty in
189 the adjusted MMLEA projections. These estimates also depend on the models simulating a
190 realistic forced NAO response; Section 4 discusses this further.

191 Now we ask to what extent the NAO explains uncertainty in North Atlantic circulation
192 projections due to IV. Figure 2 presents for each MMLEA model a decomposition of the total

193 ensemble spread in MSLP (top row) into an NAO-congruent part (second row) and a residual
194 (third row). The total uncertainty from IV is generally largest at high northern latitudes,
195 extending from Greenland to Northern Europe, as well as in the central North Atlantic. There is
196 also larger uncertainty from IV in north-eastern North America and continental Europe. The
197 NAO contributes to a large proportion (>50%; Figure 2, bottom row) of the uncertainty in MSLP
198 projections at high latitudes, and a substantial proportion (up to 50%) of the uncertainty around
199 the Mediterranean region. The large residual uncertainty in projections in the central Atlantic and
200 western Europe is largely associated with the East Atlantic (EA) pattern (Figure S2), the second
201 dominant mode of circulation variability in the North Atlantic sector (Barnston & Livezey, 1987;
202 Moore et al., 2011; Wallace & Gutzler, 1981).

203 3.2 Uncertainty in the forced response

204 Figure 1 shows structural differences in the late 21st century forced NAO response across
205 the MMLEA models. Here we ask: when do the forced NAO response and model structural
206 differences in the response become detectable from IV? In the early-to-mid 21st century, most
207 individual model responses are small and non-robust (Figure 3a-b). GFDL-ESM2M is one
208 exception, having a relatively large and robust positive NAO response by 2020-2039. By 2060-
209 2079, most of the model responses become large enough to be detected from IV, except for EC-
210 EARTH due to its smaller response and ensemble size (Figure 3c). Regarding detection of model
211 differences in response, in the mid-21st century only GFDL-ESM2M is robustly distinguishable
212 from the other models (Figure 3b). By 2060-2079, the only model with a negative NAO response
213 (CanESM2; Böhnisch et al., 2020) becomes distinct from other models (Figure 3c). By 2080-
214 2099, CSIRO-Mk3.6 and MPI-ESM-LR develop stronger positive responses and become distinct
215 from CESM1-CAM5 and EC-EARTH (Figure 3d). In short, most of the models simulate a robust
216 forced NAO response by 2060-2079. However, most inter-model differences in the forced
217 response are only detectable by 2080-2099, when % U_{MD} first dominates over % U_{IV} (Figure 3a-
218 d). This largely holds when the model-based IV estimates are adjusted to an observation-based
219 estimate (Figure S3).

220 We now calculate the minimum ensemble size (N_{min}) required to robustly detect a forced
221 NAO index response, and model differences in this response, given a certain magnitude of IV.

222 First, note that N_{\min} is larger when identifying differences in forced response between models
223 than when identifying a response of equivalent magnitude in one model (Figure 3e-f). This is
224 consistent with inter-model differences in forced response emerging from IV later. An NAO
225 index response of 0.5 hPa – typical of early-to-mid 21st century MMLEA responses (Figure 3a-b)
226 – requires $N_{\min}=10, 20$ or 40 to detect in a model with low (2.5th percentile), median, or high
227 (97.5th percentile) IV, basing the IV magnitude on the CMIP5/6 multi-model ensemble. For
228 context, the interannual variability (standard deviation) in the DJF NAO index is ~4 hPa in the
229 observation-based datasets. N_{\min} is doubled to 20, 40 or 80 to detect a difference in NAO index
230 response of 0.5 hPa between two models. N_{\min} for a high IV model is similar to N_{\min} calculated
231 using observation-based IV estimates. All subsequent results use the high IV estimate and thus
232 provide an upper bound on N_{\min} . To detect larger NAO responses of 1 hPa and 2 hPa – typical of
233 late 21st century MMLEA responses (Figure 3c-d) – at least 15 or 5 members are required,
234 respectively. This becomes 30 or 10 members for a difference in response. The largest MMLEA
235 model response, and difference in response, of ~4 hPa in 2080-2099 (Figure 3d) requires only 3
236 members to detect. N_{\min} is first minimised at 2 for a response of 5 hPa or a difference in response
237 of 7 hPa. Therefore, when considering more realistic IV estimates, most NAO anomalies and
238 model differences in Figure 1 are non-robust in CMIP5/6 models with only 1 ensemble member.

239 Finally, we ask to what extent inter-model spread in the forced response of North Atlantic
240 circulation projects onto the NAO structure and, therefore, reflects differences in the response of
241 the NAO to external forcing. The forced MSLP response is rather different across the MMLEA
242 models (Figure 4, top row). For example, in CSIRO-Mk3.6, GFDL-ESM2M and MPI-ESM-LR
243 there is a north-south dipole in pressure anomalies, which is not present in CanESM2, CESM1-
244 CAM5 and EC-EARTH. This is associated with inter-model spread in the NAO-congruent
245 MSLP response (Figure 4, middle row). However, while a substantial portion of the forced North
246 Atlantic MSLP response is NAO-congruent in some models (e.g., 80% in GFDL-ESM2M), this
247 is not true of other models (e.g., EC-EARTH), and there are large residuals in all models (Figure
248 4, bottom row). Besides limited regions at high latitudes and in Southern Europe, the MSLP
249 residuals contribute to the majority of the inter-model spread in the forced MSLP response (e.g.,
250 see Greenland, eastern North America and central Europe; Figure 4, far-right column).

251 **4 Discussion and conclusions**

252 The results presented here have improved our understanding of North Atlantic circulation
253 projections in various ways.

254 First, while the CMIP5/6 models under RCP8.5/SSP5-8.5 show a mean response in the
255 winter NAO index of ~ 1.5 hPa during the late 21st century (2080-2099) compared to near-
256 present-day (1995-2014), the individual model responses span 6-7 hPa and less than 90% of
257 models agree on the sign of response. The MMLEA models suggest that approximately two-
258 thirds of the large inter-model spread in CMIP5/6 could be explained by potentially reducible
259 model structural differences and one-third by irreducible uncertainty from IV. While previous
260 studies have noted the large spread in North Atlantic circulation projections (Section 1), this
261 study is the first to quantify these sources of uncertainty using large initial-condition ensembles
262 performed by a subset of CMIP5 models. The real-world relevance of this separation relies on
263 models correctly reproducing the observed magnitude of low frequency IV and forced NAO
264 response. We find the former is generally underestimated in models as in previous studies, but
265 note the latter may also be underestimated (see below).

266 Second, as expected from the relatively large IV of the winter NAO, we find a relatively
267 long time horizon for detecting a forced NAO response. The MMLEA models suggest that the
268 forced NAO response is only detectable from IV by 2060-2079 and that model structural
269 uncertainty in the forced response is detectable by 2080-2099. Uncertainty in NAO projections is
270 therefore largely irreducible for most of the 21st century. While individual MMLEA models have
271 larger NAO responses that are distinct from IV and other models earlier, this is generally not the
272 case. This highlights a benefit of using the new MMLEA archive here, whereas previous studies
273 have been limited to using a single-model large initial-condition ensemble to quantify the time of
274 emergence of a forced circulation response (Deser et al., 2012, 2017).

275 Third, we show that a relatively large ensemble size is required to robustly separate the
276 forced NAO response, and model differences in this response, from IV. A typical response (or
277 model difference) of 1-2 hPa over the 21st century requires at least 15-5 (30-10) ensemble
278 members to detect based on realistic estimates of IV. Even for very large responses (model
279 differences) of around 5 hPa (7 hPa), 2 members are required for detection – meaning the

280 majority of model responses and differences are non-robust in CMIP5/6 models with only 1
281 ensemble member. This result is relevant to the growing application of emergent constraint
282 techniques for narrowing uncertainty in future projections, as this relies on knowledge of the
283 forced response and differences in forced responses across ensembles of models. Future model
284 intercomparison experiment designs should consider the required ensemble sizes for examining
285 regional climate signals (e.g., Milinski et al., 2020).

286 Finally, we have examined the extent to which the spread in North Atlantic MSLP
287 projections is NAO-congruent. Regarding spread from IV, this is large in most North Atlantic
288 regions and surrounding land areas, where the NAO explains over 50% of the inter-member
289 spread in individual MMLEA models at higher latitudes and up to 50% around the
290 Mediterranean region. The residual spread in the central Atlantic and western Europe is largely
291 explained by the EA pattern. That the spread in projections from IV is largely explained by
292 dominant modes of atmospheric variability agrees with Deser et al. (2012). These results build
293 on those of Deser et al. (2017), who only analysed the NAO contribution to spread in projections
294 from IV.

295 Regarding inter-model spread in the forced North Atlantic MSLP response, while this is
296 largely NAO-congruent at high latitudes and in Southern Europe, the majority of the spread is
297 not NAO-congruent. Therefore, improving understanding of the NAO alone may not constrain
298 the reducible uncertainty in North Atlantic MSLP projections. This is surprising considering
299 previous work demonstrating the resemblance of externally forced model responses to the
300 dominant modes of IV (Deser et al., 2004, 2012). The large residual uncertainty in the forced
301 MSLP response over Greenland may be associated with local near-surface temperature changes
302 over orography and/or the extrapolation of pressure to mean sea level.

303 These results have some limitations. First, MSLP only provides one perspective of the
304 circulation. When using the zonal wind at 850 hPa (U850), which is related to the meridional
305 pressure gradient, we find a shift in the regions with large uncertainty from IV (Figure S4).
306 Furthermore, inter-model spread in the forced U850 response appears more NAO-congruent over
307 Europe than for MSLP (Figure S5).

308 Second, models appear to underestimate predictable forced NAO variations by a factor of
309 2 on seasonal timescales (Baker et al., 2018; Dunstone et al., 2016; Eade et al., 2014; Scaife et
310 al., 2014; Scaife & Smith, 2018) and by a factor of 10 on decadal timescales (Smith et al., 2020).
311 This issue may also affect multi-decadal NAO projections, though given the limited temporal
312 extent of the observational record this is difficult to assess. If it does, this implies an
313 underestimation of model differences in the forced NAO response and therefore the contribution
314 of the NAO to inter-model spread in the forced circulation response, as well as an overestimation
315 of the time horizon and “true” ensemble size required to detect a forced NAO response from IV.
316 A further limitation of our analysis is that the MMLEA models may not span the full range of
317 forced NAO responses in the CMIP5/6 models. However, it is difficult to assess this given the
318 small ensemble sizes for most CMIP5/6 models.

319 The dynamical mechanisms responsible for inter-model spread in the forced North
320 Atlantic circulation response need to be understood to identify potential physical constraints on
321 the spread. Oudar et al. (2020) identified various mechanisms within CMIP5/6 projections, but
322 could not determine which are relevant for spread from IV and/or model differences. Harvey et
323 al. (2020)’s results suggest that mean state biases in the North Atlantic jet do not provide a useful
324 constraint. Future studies could utilise MMLEA to investigate the dynamical mechanisms
325 further.

326 **Figure 1. Projections of the DJF NAO index for [2080-2099]–[1995-2014] in the CMIP6,**
 327 **CMIP5 and MMLEA models.** For CMIP5/6 models, ensemble means are shown if more than
 328 one ensemble member is available. Hatching indicates a CMIP5/6 model anomaly that is larger
 329 than 2 standard deviations of model-specific IV (Text S3). Darker cyan/blue bars indicate the
 330 MMM. Whiskers for MMLEA models indicate the 2.5-97.5% range of responses across the
 331 ensemble members. Section 2.1 describes the model forcing scenarios. Grey lines show the 2.5-
 332 97.5% range of 10^5 differences in 20-year epoch means of different observation-based records
 333 (Section 2.1), selected by randomly resampling with replacement. Grey shaded box shows this
 334 range for Obs LE. The observation-based IV estimates are shifted by the CMIP6 MMM anomaly
 335 for comparison with the inter-model spread.

336 **Figure 2. Inter-member variance in projections of DJF MSLP for [2080-2099]–[1995-2014]**
 337 **for each MMLEA model.** [Top row] Total (σ_{tot}^2); [Second row] NAO-congruent part (σ_{nao}^2);
 338 [Third row] Residual (σ_{res}^2); [Bottom row] Proportion of total variance explained by NAO. σ_{nao}^2
 339 is obtained by regressing the total inter-member spread in MSLP on the spread in NAO-
 340 congruent MSLP at each grid-point. σ_{res}^2 is the variance in the residuals of this regression.

341 **Figure 3. Detecting a forced response in DJF NAO index and inter-model differences in this**
 342 **response. a-d,** NAO anomalies in MMLEA models for future 20-year epochs (1995-2014
 343 baseline). Whiskers are 95% confidence intervals and numbers indicate ensemble size. Section
 344 2.3 defines % U_{IV} and % U_{MD} . **e,** N_{min} required to detect a forced NAO response of a given
 345 magnitude at the 95% confidence level based on IV estimates from MMLEA models, CMIP5/6
 346 models, and observation-based datasets (Text S2-S3). **f,** As in **e** but for detecting a difference in
 347 forced response; note different y-axis scale. Single CMIP5/6 models can be located within the
 348 grey plumes using Table S2.

349 **Figure 4. Projections of ensemble mean DJF MSLP for [2080-2099]–[1995-2014] for each**
 350 **MMLEA model, and their inter-model variance.** [Top] Total; [Middle] NAO-congruent part;
 351 [Bottom] Residual. r^2 is the squared area-weighted pattern correlation between the total response
 352 and the NAO-congruent part.

353 Acknowledgments

354 CMM and ACM were supported by the European Union's Horizon 2020 research and innovation
355 programme under grant agreement No 820829 (CONSTRAIN project). ACM was supported by a
356 NERC Independent Research Fellowship (NE/M018199/1) and The Leverhulme Trust (PLP-
357 2018-278). We are grateful to Isla Simpson, Clara Deser, Flavio Lehner and John Fyfe for useful
358 discussions about the MMLEA dataset and North Atlantic variability. We thank the
359 CONSTRAIN project community for useful comments on this work and two anonymous
360 reviewers for their constructive comments which improved the manuscript. We acknowledge the
361 U.S. CLIVAR Working Group on Large Ensembles for providing the Multi-Model Large
362 Ensemble Archive and Observational Large Ensemble data. We acknowledge the World Climate
363 Research Programme, which, through its Working Group on Coupled Modelling, coordinated
364 and promoted CMIP5/6. We thank the climate modelling groups for producing and making
365 available their model output; the Earth System Grid Federation (ESGF) and UK Centre for
366 Environmental Data Analytics (CEDA) JASMIN cluster for archiving the data and providing
367 access; and the multiple funding agencies who support CMIP5/6, ESGF and CEDA/JASMIN.

368

369 Data availability statement

370 The Multi-Model Large Ensemble Archive and Observational Large Ensemble data can be
371 accessed at <http://www.cesm.ucar.edu/projects/community-projects/MMLEA/>. The GFDL-
372 ESM2M large ensemble data used here can be accessed from the Princeton Large Ensemble
373 Archive through Globus (<https://www.sarahschlunegger.com/large-ensemble-archive>). The
374 CMIP5 and CMIP6 datasets were downloaded from CEDA/JASMIN (timestamps of 21-23
375 September 2020 and 4 December 2020, respectively); these are publicly available through the
376 Earth System Grid Federation at <https://esgf-index1.ceda.ac.uk/projects/esgf-ceda/>. The
377 observational datasets can be downloaded from
378 https://psl.noaa.gov/data/gridded/data.20thC_ReanV3.html (20CRv3) and
379 <https://www.ecmwf.int/en/forecasts/datasets/reanalysis-datasets/era-20c> (ERA20C).

380 **References**

- 381 Ambaum, M. H. P., Hoskins, B. J., & Stephenson, D. B. (2001). Arctic Oscillation or North
382 Atlantic Oscillation? *Journal of Climate*, *14*(16), 3495–3507.
383 [https://doi.org/10.1175/1520-0442\(2001\)014<3495:AOONAO>2.0.CO;2](https://doi.org/10.1175/1520-0442(2001)014<3495:AOONAO>2.0.CO;2)
- 384 Baker, L. H., Shaffrey, L. C., Sutton, R. T., Weisheimer, A., & Scaife, A. A. (2018). An
385 intercomparison of skill and overconfidence/underconfidence of the wintertime North
386 Atlantic Oscillation in multimodel seasonal forecasts. *Geophysical Research Letters*, *45*,
387 7808–7817. <https://doi.org/10.1029/2018GL078838>
- 388 Barnston, A. G., & Livezey, R. E. (1987). Classification, seasonality and persistence of low-
389 frequency atmospheric circulation patterns. *Monthly Weather Review*, *115*(6), 1083–
390 1126. [https://doi.org/10.1175/1520-0493\(1987\)115<1083:CSAPOL>2.0.CO;2](https://doi.org/10.1175/1520-0493(1987)115<1083:CSAPOL>2.0.CO;2)
- 391 Böhnisch, A., Ludwig, R., & Leduc, M. (2020). Using a nested single-model large ensemble to
392 assess the internal variability of the North Atlantic Oscillation and its climatic
393 implications for central Europe. *Earth System Dynamics*, *11*, 617–640.
394 <https://doi.org/10.5194/esd-11-617-2020>
- 395 Bracegirdle, T. J., Lu, H., Eade, R., & Woollings, T. (2018). Do CMIP5 models reproduce
396 observed low-frequency North Atlantic jet variability? *Geophysical Research Letters*, *45*,
397 7204–7212. <https://doi.org/10.1029/2018GL078965>
- 398 Buehler, T., Raible, C. C., & Stocker, T. F. (2011). The relationship of winter season North
399 Atlantic blocking frequencies to extreme cold or dry spells in the ERA-40. *Tellus A:
400 Dynamic Meteorology and Oceanography*, *63*(2), 174–187.
401 <https://doi.org/10.1111/j.1600-0870.2010.00492.x>
- 402 Collins, M., Knutti, R., Arblaster, J., Dufresne, J.-L., Fichet, T., Friedlingstein, P., et al. (2013).
403 Long-term Climate Change: Projections, Commitments and Irreversibility. In T. F.
404 Stocker, et al. (Eds.), *Climate Change 2013: The Physical Science Basis. Contribution of
405 Working Group I to the Fifth Assessment Report of the Intergovernmental Panel on*

- 406 *Climate Change* (pp. 1029–1136). Cambridge, UK, and New York: Cambridge
407 University Press. <https://doi.org/10.1017/CBO9781107415324.024>
- 408 Compo, G. P., Whitaker, J. S., Sardeshmukh, P. D., Matsui, N., Allan, R. J., Yin, X., et al.
409 (2011). The Twentieth Century Reanalysis Project. *Quarterly Journal of the Royal*
410 *Meteorological Society*, 137, 1–28. <http://dx.doi.org/10.1002/qj.776>
- 411 Deser, C., Hurrell, J. W., & Phillips, A. S. (2017). The role of the North Atlantic Oscillation in
412 European climate projections. *Climate Dynamics*, 49, 3141–3157.
413 <https://doi.org/10.1007/s00382-016-3502-z>
- 414 Deser, C., Lehner, F., Rodgers, K. B., Ault, T., Delworth, T. L., DiNezio, P. N., et al. (2020).
415 Insights from Earth system model initial-condition large ensembles and future prospects.
416 *Nature Climate Change*, 10, 277–286. <https://doi.org/10.1038/s41558-020-0731-2>
- 417 Deser, C., Magnusdottir, G., Saravanan, R., & Phillips, A. (2004). The Effects of North Atlantic
418 SST and Sea Ice Anomalies on the Winter Circulation in CCM3. Part II: Direct and
419 Indirect Components of the Response. *Journal of Climate*, 17(5), 877–889.
420 [https://doi.org/10.1175/1520-0442\(2004\)017<0877:TEONAS>2.0.CO;2](https://doi.org/10.1175/1520-0442(2004)017<0877:TEONAS>2.0.CO;2)
- 421 Deser, C., Phillips, A., Bourdette, V., & Teng, H. (2012). Uncertainty in climate change
422 projections: the role of internal variability. *Climate Dynamics*, 38, 527–546.
423 <https://doi.org/10.1007/s00382-010-0977-x>
- 424 Dommenges, D., & Latif, M. (2002). A Cautionary Note on the Interpretation of EOFs. *Journal*
425 *of Climate*, 15(2), 216–225.
426 [https://doi.org/10.1175/1520-0442\(2002\)015%3c0216:ACNOTI%3e2.0.CO;2](https://doi.org/10.1175/1520-0442(2002)015%3c0216:ACNOTI%3e2.0.CO;2)
- 427 Dunstone, N., Smith, D., Scaife, A., Hermanson, L., Eade, R., Robinson, N., et al. (2016). Skilful
428 predictions of the winter North Atlantic Oscillation one year ahead. *Nature Geoscience*,
429 9, 809–814. <https://doi.org/10.1038/ngeo2824>
- 430 Eade, R., Smith, D., Scaife, A., Wallace, E., Dunstone, N., Hermanson, L., & Robinson, N.
431 (2014). Do seasonal-to-decadal climate predictions underestimate the predictability of the

- 432 real world? *Geophysical Research Letters*, 41, 5620–5628.
433 <https://doi.org/10.1002/2014GL061146>
- 434 Eyring, V., Bony, S., Meehl, G. A., Senior, C. A., Stevens, B., Stouffer, R. J., & Taylor, K. E.
435 (2016). Overview of the Coupled Model Intercomparison Project Phase 6 (CMIP6)
436 experimental design and organization. *Geoscientific Model Development*, 9, 1937–1958.
437 <https://doi.org/10.5194/gmd-9-1937-2016>
- 438 Harvey, B. J., Cook, P., Shaffrey, L. C., & Schiemann, R. (2020). The response of the northern
439 hemisphere storm tracks and jet streams to climate change in the CMIP3, CMIP5, and
440 CMIP6 climate models. *Journal of Geophysical Research: Atmospheres*, 125,
441 e2020JD032701. <https://doi.org/10.1029/2020JD032701>
- 442 Harvey, B. J., Shaffrey, L. C., & Woollings, T. J. (2014). Equator-to-pole temperature
443 differences and the extra-tropical storm track responses of the CMIP5 climate models.
444 *Climate Dynamics*, 43, 1171–1182. <https://doi.org/10.1007/s00382-013-1883-9>
- 445 Hawkins, E., & Sutton, R. (2009). The Potential to Narrow Uncertainty in Regional Climate
446 Predictions. *Bulletin of the American Meteorological Society*, 90(8), 1095–1108.
447 <https://doi.org/10.1175/2009BAMS2607.1>
- 448 Hazeleger, W., Severijns, C., Semmler, T., Ștefănescu, S., Yang, S., Wang, X., et al. (2010). EC-
449 Earth. *Bulletin of the American Meteorological Society*, 91(10), 1357–1364.
450 <https://doi.org/10.1175/2010BAMS2877.1>
- 451 Hurrell, J. W., Kushnir, Y., Ottersen, G., & Visbeck, M. (2003). An overview of the North
452 Atlantic Oscillation. In J. W. Hurrell, Y. Kushner, G. Ottersen, & M. Visbeck (Eds.), *The*
453 *North Atlantic Oscillation: Climate Significance and Environmental Impact*, *Geophysical*
454 *Monograph Series* (Vol. 134, pp. 1–35). Washington, DC: American Geophysical Union.
455 <https://doi.org/10.1029/134GM01>
- 456 Jeffrey, S., Rotstayn, L., Collier, M., Dravitzki, S., Hamalainen, C., Moeseneder, C., et al.
457 (2013). Australia's CMIP5 submission using the CSIRO-Mk3.6 model. *Australian*

- 458 *Meteorological and Oceanographic Journal*, 63(1), 1–13.
459 <https://doi.org/10.22499/2.6301.001>
- 460 Kay, J. E., Deser, C., Phillips, A., Mai, A., Hannay, C., Strand, G., et al. (2015). The Community
461 Earth System Model (CESM) Large Ensemble Project: A Community Resource for
462 Studying Climate Change in the Presence of Internal Climate Variability. *Bulletin of the*
463 *American Meteorological Society*, 96(8), 1333–1349. [https://doi.org/10.1175/BAMS-D-](https://doi.org/10.1175/BAMS-D-13-00255.1)
464 [13-00255.1](https://doi.org/10.1175/BAMS-D-13-00255.1)
- 465 Kim, W. M., Yeager, S., Chang, P., & Danabasoglu, G. (2018). Low-Frequency North Atlantic
466 Climate Variability in the Community Earth System Model Large Ensemble. *Journal of*
467 *Climate*, 31(2), 787–813. <https://doi.org/10.1175/JCLI-D-17-0193.1>
- 468 Kirchmeier-Young, M. C., Zwiers, F. W., & Gillett, N. P. (2016). Attribution of extreme events
469 in Arctic sea ice extent. *Journal of Climate*, 30(2), 553–571.
470 <https://doi.org/10.1175/JCLI-D-16-0412.1>
- 471 Kravtsov, S. (2017). Pronounced differences between observed and CMIP5-simulated
472 multidecadal climate variability in the twentieth century. *Geophysical Research Letters*,
473 44, 5749–5757. <https://doi.org/10.1002/2017GL074016>
- 474 Maher, N., Milinski, S., Suarez-Gutierrez, L., Botzet, M., Dobrynin, M., Kornblueh, L., &
475 Marotzke, J. (2019). The Max Planck Institute grand ensemble: Enabling the exploration
476 of climate system variability. *Journal of Advances in Modeling Earth Systems*, 11, 2050–
477 2069. <https://doi.org/10.1029/2019MS001639>
- 478 Maher, N., Power, S. B. & Marotzke, J. (2021). More accurate quantification of model-to-model
479 agreement in externally forced climatic responses over the coming century. *Nature*
480 *Communications*, 12, 788. <https://doi.org/10.1038/s41467-020-20635-w>
- 481 Manzini, E., Karpechko, A. Y., Anstey, J., Baldwin, M. P., Black, R. X., Cagnazzo, C., et al.
482 (2014). Northern winter climate change: Assessment of uncertainty in CMIP5 projections
483 related to stratosphere-troposphere coupling. *Journal of Geophysical Research:*
484 *Atmospheres*, 119, 7979–7998. <https://doi.org/10.1002/2013JD021403>

- 485 McKinnon, K. A., & Deser, C. (2018). Internal Variability and Regional Climate Trends in an
486 Observational Large Ensemble. *Journal of Climate*, *31*(17), 6783–6802.
487 <https://doi.org/10.1175/JCLI-D-17-0901.1>
- 488 Meinshausen, M., Nicholls, Z. R. J., Lewis, J., Gidden, M. J., Vogel, E., Freund, M., et al.
489 (2020). The shared socio-economic pathway (SSP) greenhouse gas concentrations and
490 their extensions to 2500. *Geoscientific Model Development*, *13*, 3571–3605.
491 <https://doi.org/10.5194/gmd-13-3571-2020>
- 492 Meinshausen, M., Smith, S. J., Calvin, K., Daniel, J. S., Kainuma, M. L. T., Lamarque, J.-F., et
493 al. (2011). The RCP greenhouse gas concentrations and their extensions from 1765 to
494 2300. *Climatic Change*, *109*, 213. <https://doi.org/10.1007/s10584-011-0156-z>
- 495 Milinski, S., Maher, N., & Olonscheck, D. (2020). How large does a large ensemble need to be?
496 *Earth System Dynamics*, *11*, 885–901. <https://doi.org/10.5194/esd-11-885-2020>
- 497 Moore, G. W. K., Pickart, R. S., & Renfrew, I. A. (2011). Complexities in the climate of the
498 subpolar North Atlantic: a case study from the winter of 2007. *Quarterly Journal of the*
499 *Royal Meteorological Society*, *137*, 757–767. <https://doi.org/10.1002/qj.778>
- 500 Oudar, T., Cattiaux, J., & Douville, H. (2020). Drivers of the northern extratropical eddy-driven
501 jet change in CMIP5 and CMIP6 models. *Geophysical Research Letters*, *47*,
502 e2019GL086695. <https://doi.org/10.1029/2019GL086695>
- 503 Poli, P., Hersbach, H., Dee, D. P., Berrisford, P., Simmons, A. J., Vitart, F., et al. (2016). ERA-
504 20C: An Atmospheric Reanalysis of the Twentieth Century. *Journal of Climate*, *29*(11),
505 4083–4097. <https://doi.org/10.1175/JCLI-D-15-0556.1>
- 506 Rodgers, K. B., Lin, J., & Frölicher, T. L. (2015). Emergence of multiple ocean ecosystem
507 drivers in a large ensemble suite with an Earth system model. *Biogeosciences*, *12*(11),
508 3301–3320. <https://doi.org/10.5194/bg-12-3301-2015>
- 509 Scaife, A. A., Arribas, A., Blockley, E., Brookshaw, A., Clark, R. T., Dunstone, N., et al. (2014).
510 Skillful long-range prediction of European and North American winters. *Geophysical*
511 *Research Letters*, *41*, 2514–2519. <https://doi.org/10.1002/2014GL059637>

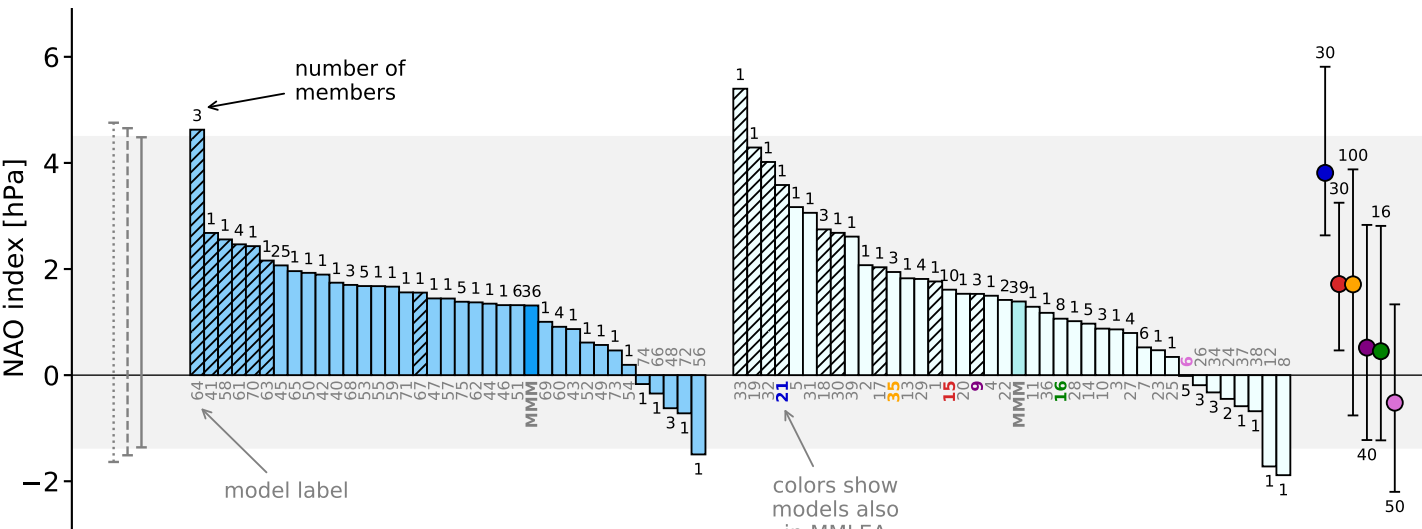
- 512 Scaife, A. A., & Smith, D. (2018). A signal-to-noise paradox in climate science. *npj Climate and*
513 *Atmospheric Science*, *1*, 28. <https://doi.org/10.1038/s41612-018-0038-4>
- 514 Schlunegger, S., Rodgers, K. B., Sarmiento, J. L., Frölicher, T. L., Dunne, J. P., Ishii, M., et al.
515 (2019). Emergence of anthropogenic signals in the ocean carbon cycle. *Nature Climate*
516 *Change*, *9*, 719–725. <https://doi.org/10.1038/s41558-019-0553-2>
- 517 Screen, J. A., Deser, C., Simmonds, I., & Tomas, R. (2014). Atmospheric impacts of Arctic sea-
518 ice loss, 1979–2009: separating forced change from atmospheric internal variability.
519 *Climate Dynamics*, *43*, 333–344. <https://doi.org/10.1007/s00382-013-1830-9>
- 520 Shepherd, T. (2014). Atmospheric circulation as a source of uncertainty in climate change
521 projections. *Nature Geoscience*, *7*, 703–708. <https://doi.org/10.1038/ngeo2253>
- 522 Simpson, I. R., Bacmeister, J., Neale, R. B., Hannay, C., Gettelman, A., Garcia, R. R., et al.
523 (2020). An evaluation of the large-scale atmospheric circulation and its variability in
524 CESM2 and other CMIP models. *Journal of Geophysical Research: Atmospheres*, *125*,
525 e2020JD032835. <https://doi.org/10.1029/2020JD032835>
- 526 Simpson, I. R., Deser, C., McKinnon, K. A., & Barnes, E. A. (2018). Modeled and Observed
527 Multidecadal Variability in the North Atlantic Jet Stream and Its Connection to Sea
528 Surface Temperatures. *Journal of Climate*, *31*(20), 8313–8338.
529 <https://doi.org/10.1175/JCLI-D-18-0168.1>
- 530 Simpson, I. R., Hitchcock, P., Seager, R., Wu, Y., & Callaghan, P. (2018). The Downward
531 Influence of Uncertainty in the Northern Hemisphere Stratospheric Polar Vortex
532 Response to Climate Change. *Journal of Climate*, *31*(16), 6371–6391.
533 <https://doi.org/10.1175/JCLI-D-18-0041.1>
- 534 Slivinski, L. C., Compo, G. P., Whitaker, J. S., Sardeshmukh, P. D., Giese, B. S., McColl, C., et
535 al. (2019). Towards a more reliable historical reanalysis: Improvements for version 3 of
536 the Twentieth Century Reanalysis system. *Quarterly Journal of the Royal Meteorological*
537 *Society*, *145*, 2876–2908. <https://doi.org/10.1002/qj.3598>

- 538 Smith, D. M., Scaife, A. A., Eade, R., Athanasiadis, P., Bellucci, A., Bethke, I., et al. (2020).
539 North Atlantic climate far more predictable than models imply. *Nature*, 583, 796–800.
540 <https://doi.org/10.1038/s41586-020-2525-0>
- 541 Stephenson, D., Pavan, V., Collins, M., Junge, M., Quadrelli, R., et al. (2006). North Atlantic
542 Oscillation response to transient greenhouse gas forcing and the impact on European
543 winter climate: A CMIP2 multi-model assessment. *Climate Dynamics*, 27(4), 401–420.
544 <https://doi.org/10.1007/s00382-006-0140-x>
- 545 Sun, L., Alexander, M., & Deser, C. (2018). Evolution of the Global Coupled Climate Response
546 to Arctic Sea Ice Loss during 1990–2090 and Its Contribution to Climate Change.
547 *Journal of Climate*, 31(19), 7823–7843. <https://doi.org/10.1175/JCLI-D-18-0134.1>
- 548 Taylor, K. E., Stouffer, R. J., & Meehl, G. A. (2012). An Overview of CMIP5 and the
549 Experiment Design. *Bulletin of the American Meteorological Society*, 93(4), 485–498.
550 <https://doi.org/10.1175/BAMS-D-11-00094.1>
- 551 von Storch, H., & Zwiers, F. W. (1999). *Statistical Analysis in Climate Research*. Cambridge,
552 UK: Cambridge University Press. <https://doi.org/10.1017/CBO9780511612336>
- 553 Wallace, J. M., & Gutzler, D. S. (1981). Teleconnections in the geopotential height field during
554 the Northern Hemisphere winter. *Monthly Weather Review*, 109(4), 784–812.
555 [https://doi.org/10.1175/1520-0493\(1981\)109<0784:TITGHF>2.0.CO;2](https://doi.org/10.1175/1520-0493(1981)109<0784:TITGHF>2.0.CO;2)
- 556 Wang, X., Li, J., Sun, C., & Liu, T. (2017). NAO and its relationship with the Northern
557 Hemisphere mean surface temperature in CMIP5 simulations. *Journal of Geophysical*
558 *Research: Atmospheres*, 122, 4202–4227. <https://doi.org/10.1002/2016JD025979>
- 559 Woollings, T., Hannachi, A., & Hoskins, B. (2010). Variability of the North Atlantic eddy-driven
560 jet stream. *Quarterly Journal of the Royal Meteorological Society*, 136, 856–868.
561 <https://doi.org/10.1002/qj.625>
- 562 Zappa, G., Pithan, F., & Shepherd, T. G. (2018). Multimodel evidence for an atmospheric
563 circulation response to Arctic sea ice loss in the CMIP5 future projections. *Geophysical*
564 *Research Letters*, 45, 1011–1019. <https://doi.org/10.1002/2017GL076096>

565 Zappa, G., & Shepherd, T. G. (2017). Storylines of Atmospheric Circulation Change for
566 European Regional Climate Impact Assessment. *Journal of Climate*, 30(16), 6561–6577.
567 <https://doi.org/10.1175/JCLI-D-16-0807.1>

Figure 1.

Projections of the DJF NAO index for [2080-2099] – [1995-2014]



⋮	ERA20C	●	GFDL-ESM2M	●	CESM1-CAM5	I	2.5-97.5% range
⋮	20CRv3	●	CSIRO-Mk3.6	●	EC-EARTH	○	Ensemble mean
I	Obs LE	●	MPI-ESM-LR	●	CanESM2		

Figure 2.

Inter-member variance in DJF MSLP for [2080-2099] – [1995-2014]

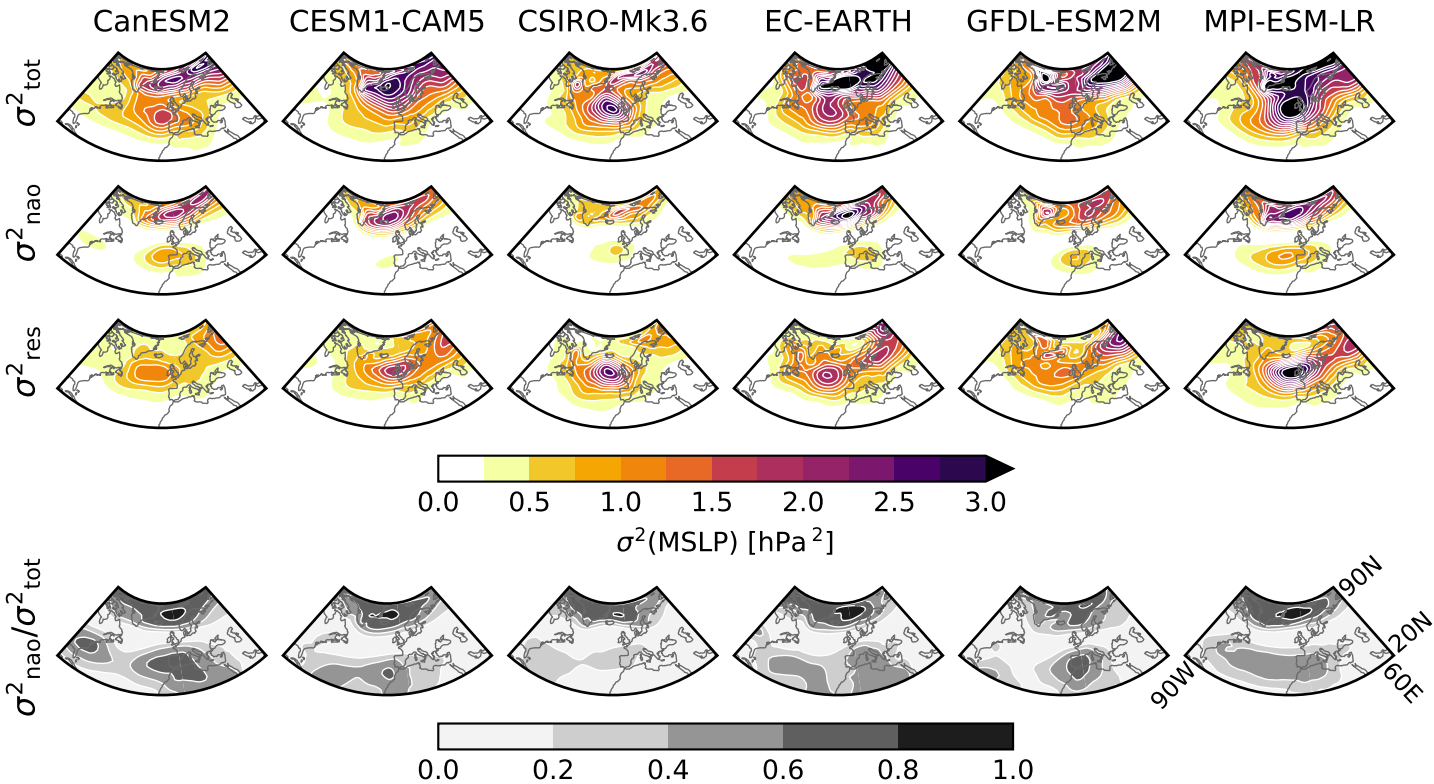


Figure 3.

Detecting forced differences in the DJF NAO index

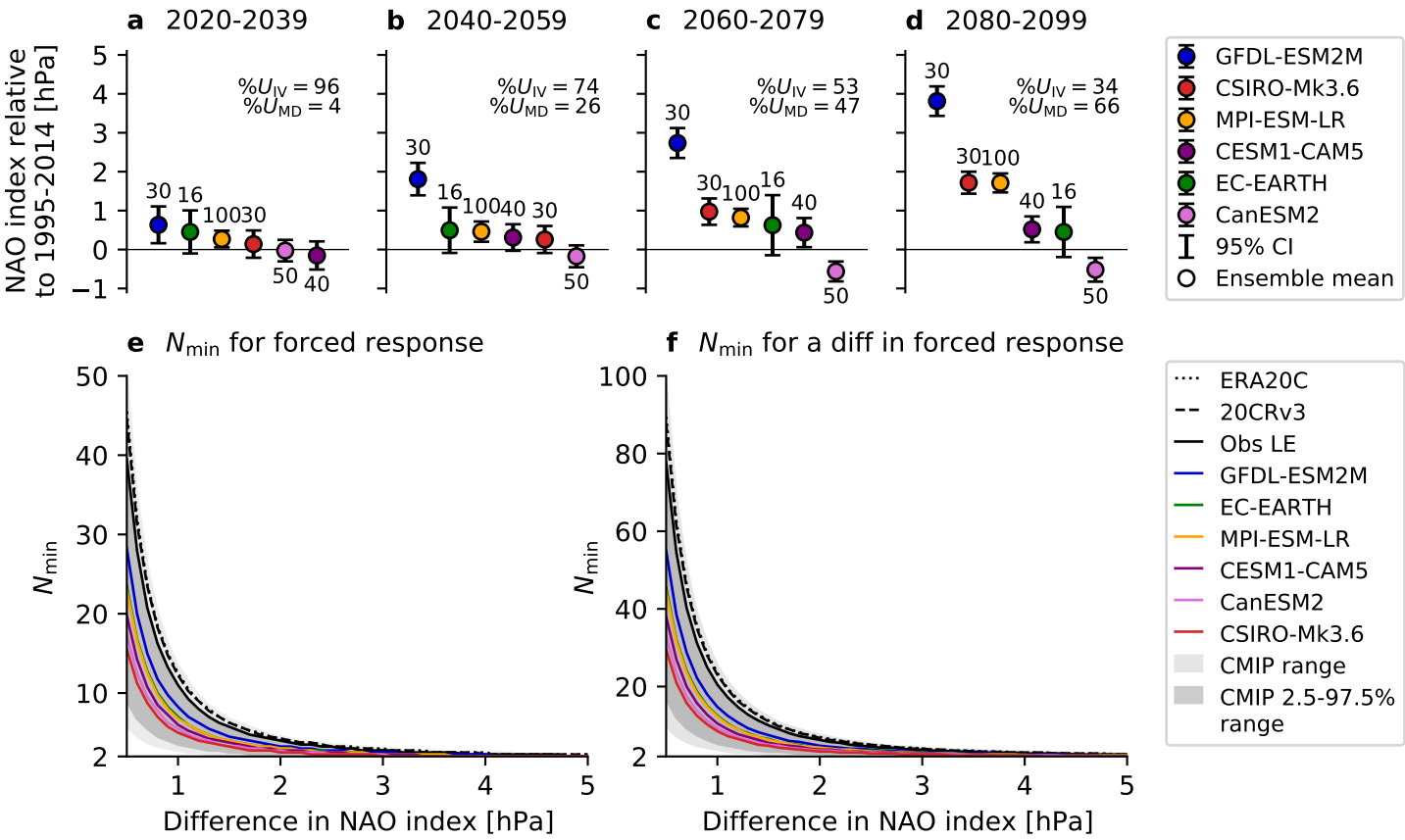


Figure 4.

Ensemble mean DJF MSLP for [2080-2099] – [1995-2014]

